PERGAMON

International Journal of Multiphase Flow 27 (2001) 147–170

International Journal of Multiphase Flow

www.elsevier.com/locate/ijmulflow

Subchannel void-fraction measurements in a 6×6 rod bundle using a simple gamma-transmission method

H.V. Kok[a], T.H.J.J. van der Hagen[a,b,*], R.F. Mudde[b]

[a]*Interfaculty Reactor Institute, Delft University of Technology, Mekelweg 15, 2629 JB Delft, The Netherlands*
[b]*Kramers Laboratorium voor Fysische Technologie, Delft University of Technology, Pr. Bernhardlaan 6, 2628 BW, Delft, The Netherlands*

Received 13 March 1999; received in revised form 28 December 1999

Abstract

A relatively simple subchannel void-fraction measurement system was developed and applied to a scaled model of a BWR fuel assembly. The measurement system is based upon the gamma-transmission technique and uses a tomographic reconstruction procedure to calculate the void-fractions in the subchannels. Data pre-processing is used to remove positioning errors of the gamma source and detector. Measurements are performed under different operating conditions and radial power profiles. The measurements are compared with the drift-flux two-phase flow model. The void-fraction in the wall and corner subchannels is lower than average. By applying the drift-flux model to each subchannel separately and comparing this calculation with measurements the presence of lateral void-drift should be detectable. However, the data do not show evidence for lateral void-drift. By comparing two chordal void-fractions, one through the fuel rods and one in between the fuel rods, a flow pattern transition could clearly be seen between a void-fraction of 30% and 40%. © 2000 Elsevier Science Ltd. All rights reserved.

Keywords: BWR; Subchannel modeling; Void fraction; Gamma-densitometry; Tomography

1. Introduction

Subchannel analysis is a widely used tool for calculating the void-fraction and other

* Corresponding author. Tel.: +31-015-278-2105; fax: +31-015-278-6422.
E-mail address: hagen@iri.tudelft.nl (T.H.J.J. van der Hagen).

PII: S0301-9322(00)00005-7

performance factors for fuel assembly designs of Boiling Water Reactors (BWRs) (Lahey, 1990). For the development and verification of these tools experimental data is needed. A lot of experiments have been performed, ranging from studies of the interaction between two subchannels in small adiabatic test sections (Yadigaroglu and Maganas, 1995) to detailed measurements of the void-fraction distribution in a full-scale BWR assembly using X-ray tomography (Yagi et al., 1992; Inoue, 1995). All these measurements have their uses, but also their limitations. The studies of the interactions between two subchannels are useful for creating models, but cannot be used to test the models when applied to a real fuel assembly. The detailed measurements of the void-fraction using X-ray tomography were limited to the exit of the fuel assembly and are very expensive to perform. Thus, there have been few measurements which can be directly compared with predictions made by the subchannel models. The purpose of this paper is to present this type of data. To obtain these, a relatively simple and cheap method has been developed for measuring the void-fraction on a subchannel basis as a function of height using a simple gamma-transmission set-up in combination with a tomographic reconstruction procedure. The key element in the design of the system is to keep the mechanical system as simple (and inexpensive) as possible and to use data pre-processing to compensate for inaccuracies of this system. The subchannel void-fraction measuring system is applied to a scaled model of a BWR fuel assembly using Freon-12 as a coolant. This electrically heated fuel assembly is part of a natural circulation loop called DESIRE (Delft Simulated Reactor, working pressure: 11 bar, temperature: 48°C). DESIRE is described in detail in van de Graaf et al. (1994a, 1994b), Kok et al. (1995) and Kok (1998). An overview of the set up is presented in Fig. 1.

The fuel assembly consists of a stainless steel casing of $54 \times 54 \times 962$ mm with walls of 3 mm thickness. It encompasses 35 electrically heated fuel rods with a diameter of 6.35 mm and a length of 830 mm and one dummy rod (corresponding to a water rod in a BWR fuel assembly). The rods are arranged in a square 6×6 lattice with a pitch of 8.8 mm (see Fig. 2). The maximum rated power for each rod is 1.6 kW. The pitch of the resistance wire inside each fuel rod is a function of the axial position in the rod in such a way that the power profile, $P'(z)$, of the fuel rods is a cosine plus offset:

$$P'(z) = P\frac{\left(1-\frac{2}{\pi}f_{\mathrm{p}}\right)+(f_{\mathrm{p}}-1)\sin\left(z\frac{\pi}{H}\right)}{H\left(1-\frac{2}{\pi}\right)} \tag{1}$$

where f_{p} is the axial peaking factor which has the value of 1.4 for DESIRE, P is the total power and H is the height of the assembly.

The subcooled coolant, Freon-12, enters the assembly from below. Due to the heat input, a two-phase flow is generated in the assembly. Different non-uniform radial power profiles can be applied, since the fuel rods can be connected to one of six different power supplies each. Consequently, the void fraction distribution is a function of the position, both in vertical and in horizontal direction, especially for non-uniform radial power profiles. The void fraction at the outlet of the assembly can be as high as 80%. Scanning the cross-sectional area at different

heights using gamma-transmission, the void fraction can be studied in great detail inside the assembly.

2. Two-phase flow modeling

This section presents the two-phase flow models against which the measurements will be compared. The calculation of the void-fraction takes place in three steps. First, the thermodynamic equilibrium quality is calculated using a heat balance. Next, the flow quality is calculated from the thermodynamic equilibrium quality. These two qualities are equal where the flow is at thermodynamic equilibrium (i.e. everywhere except in the subcooled boiling region). Finally, the void-fraction is calculated using the drift-flux model. The thermodynamic

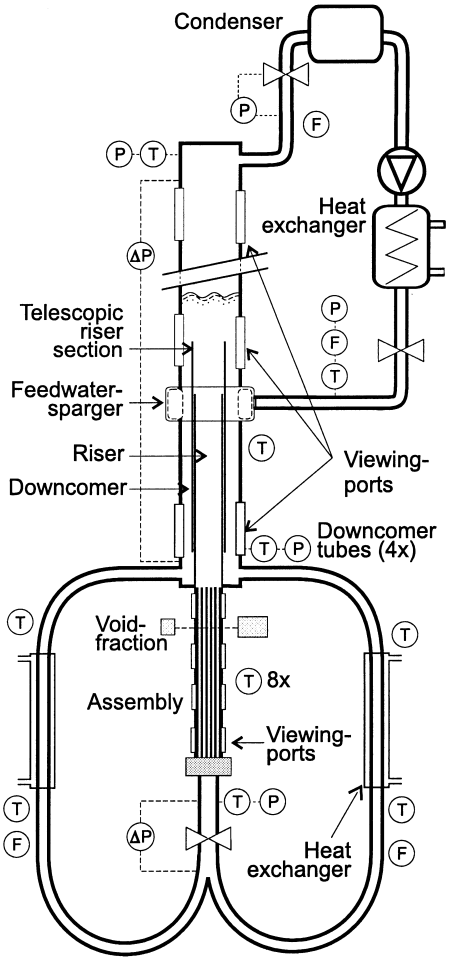

Fig. 1. Overview of the DESIRE facility (not to scale). T = thermocouple, P = pressure transducer, ΔP = differential pressure transducer, F = flow meter.

equilibrium quality, x_{eq}, is straightforward to calculate in the assembly:

$$x_{eq}(z) = -\frac{c_l T_{sub}}{h_{ev}} + \frac{1}{h_{ev}\Phi}\int_0^z P'(z)\,dz \tag{2}$$

with T_{sub} the subcooling, Φ the mass flow rate, c_l the specific heat, h_{ev} the vaporisation enthalpy and P' the linear power density. The step from thermodynamic equilibrium quality to flow quality, x, is trivial in all regions except in the subcooled boiling region. In this region, the flow quality is described using a profile-fit method. This fit gives the flow quality as a function of the equilibrium quality and the equilibrium quality at the departure point (Lahey and Moody, 1993):

$$x(z) = x_{eq}(z) - x_{eq,\,d}\exp\left(\frac{x_{eq}(z) - x_{eq,\,d}}{x_{eq,\,d}}\right) \tag{3}$$

with $x_{eq,\,d}$ the equilibrium quality at the departure point. Note that, since $x_{eq,\,d}$ is negative, $x > x_{eq}$. The development of the flow quality in the subcooled boiling region now depends only on $x_{eq,\,d}$. A correlation for the equilibrium quality at the departure point is given by Saha and Zuber (1974):

$$x_{eq,\,d} = -154\frac{\dot{q}''}{\dot{m}'' h_{ev}} \quad \text{for } N_{Pé} > 7\times 10^4 \tag{4}$$

with $\dot{q}''$ the wall heat flux and $\dot{m}''$ the mass flux. The Péclet number, $N_{Pé}$, is equal to about 1.50×10^5 under nominal conditions for DESIRE. The void-fraction, α, is calculated from the quality using the drift-flux model,

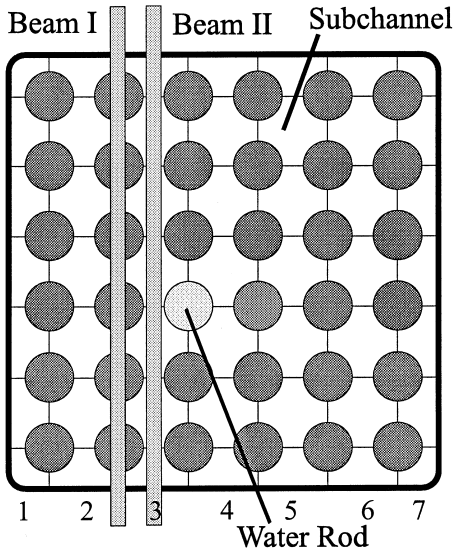

Fig. 2. Cross-section of the fuel assembly showing the subchannels and unheated 'water' rod.

$$\alpha = \frac{x}{\left(x + \frac{\rho_g}{\rho_l}(1-x)\right)\left(C_0 + \frac{v_{gj}}{\langle j \rangle}\right)} \tag{5}$$

with C_0 the distribution parameter:

$$C_0 = \frac{\langle \alpha j \rangle}{\langle \alpha \rangle \langle j \rangle} \tag{6}$$

v_{gj} the local drift velocity of the vapour:

$$v_{gj} = v_g - j \tag{7}$$

and j the volumetric flux which is defined as:

$$j = v_l(1-\alpha) + v_g\alpha \tag{8}$$

where v_l and v_g are the velocities of the liquid and gas phases, respectively. The brackets, $\langle\ \rangle$, denote an averaging operation over the channel cross-section. There are many correlations available for the distribution parameter and the local drift velocity. Dix's model was developed for rod bundles and should be applicable to DESIRE (Dix, 1971):

$$C_0 = \frac{j_g}{j}\left[1 + \left(\frac{j}{j_g} - 1\right)\left(\frac{\rho_g}{\rho_l}\right)^{0.1}\right] \tag{9}$$

$$v_{gj} = 2.9\left(\frac{g\sigma\Delta\rho}{\rho_l^2}\right)^{1/4} \tag{10}$$

with, $\Delta\rho$ as the density difference between liquid and vapour and σ as the surface tension. For a given pressure the local drift velocity in this model is a constant. For nominal pressure in DESIRE its value is 0.24 m/s.

3. Tomographic gamma-transmission technique

3.1. Gamma-transmission technique

The gamma-transmission void-fraction measurement technique is a non-intrusive and accurate method of measuring void-fractions in two-phase flows (Schrock, 1969). In the most basic application of this technique, a gamma-emitting radioactive source is placed on one side and a detector on the other side of the two-phase flow. To create a well-defined narrow beam, a collimator is placed in front of the source as well as the detector. When a material with a linear attenuation coefficient, μ, is placed between the source and the detector, the count rate, I, measured by the detector can be written as:

$$I = I_0 \, e^{-\mu d} \tag{11}$$

where I_0 is the count rate when measured in vacuum and d is the distance of the beam passing through the material. If the beam passes through several materials consecutively, for example through the liquid and vapour phases in a two phase flow, we can write:

$$I = I_0 \, e^{-\mu_m d_m} \, e^{-(\mu_l d_l + \mu_v d_v)} \tag{12}$$

where we have separated the attenuation in the structural materials, μ_m, and the attenuation in the two phases of the flow (subscript 'l' refers to the liquid phase and 'v' to the vapour phase).

Next we define the count rate for the situation that the flow is single-phase liquid, I_l, and single-phase vapour, I_v:

$$I_l = I_0 \, e^{-\mu_m d_m} \, e^{-\mu_l d}$$

$$I_v = I_0 \, e^{-\mu_m d_m} \, e^{-\mu_v d} \tag{13}$$

Combining Eqs. (12) and (13), we obtain:

$$\frac{\ln(I) - \ln(I_l)}{\ln(I_v) - \ln(I_l)} = \frac{d_v}{d} \equiv \alpha^* \tag{14}$$

with α^* the chordal void-fraction. The significance of Eq. (14) is that the chordal void-fraction determined in this way is independent of I_0 (which depends on the source strength, the distance between the source and detector and the detector efficiency), independent of μ_l and μ_v (which depend on the pressure and temperature) and independent of the attenuation in structural materials (which includes the fuel assembly casing and also the fuel rods). This means that for calibration only the two measurements made with a liquid filled and a vapour filled fuel assembly are required.

A consequence of this method is that at every location at which we want to measure the chordal void-fraction, three measurements must be performed: (i) with the assembly filled with liquid, (ii) with the assembly filled with vapour and (iii) during operation of the facility. It is essential that the source and detector are located at exactly the same position for each of these three measurements. Consequently, each time a measurement at a new position is made, the facility has to be shut down, emptied of the liquid, filled and finally started back up again. This is obviously a much cumbersome method. It is much more practical to measure the count-rates at all the desired positions once for a vapour filled assembly and once for a liquid filled assembly. Then a series of measurements be made consecutively under different operating conditions. As mentioned at the beginning of this paragraph, this does require that the source and detector can be placed accurately at the same position each time. In principle, this can be achieved with an accurate, hence expensive, mechanical positioning system. Instead of building such a system for DESIRE, we designed a simple positioning system and used data pre-processing of the measurement data to remove positioning errors.

3.2. Subchannel void-fraction measurement technique

The usual method with which tomographic reconstruction is performed is the filtered backprojection technique (see e.g. Natterer, 1982; Tanke et al., 1991). This is in essence, an inverted Fourier transform in two dimensions. This method will not work in our case because of the irregularly shaped nodes caused by the presence of the fuel rods in the assembly (see Fig. 2).

Therefore, a direct inversion method was used, which is feasible because of the limited number of nodes (49, each subchannel is considered as one node) in this problem. The method works as follows: (i) a large number of chordal void-fraction measurements are made at different angles and positions through the assembly at a specific height, (ii) for each measurement the length of the gamma beam travelled in each node is calculated. These form a matrix **A** in which the element A_{ij} is the normalized distance of beam i travelled through node j (see Fig. 3). For a specific beam Eq. (12) can be written as:

$$I = I_0 \, \mathrm{e}^{-\mu_\mathrm{m} d_\mathrm{m}} \exp\left[-\sum_j \left(\mu_\mathrm{l}(1-\alpha_j)d_j + \mu_\mathrm{v}\alpha_j d_j\right)\right] \tag{15}$$

with α_j as the average void-fraction in node j and d_j as the length of the beam in node j.

Combining Eqs. (14) and (15) gives an expression for the chordal void-fraction along

$$\alpha_i^* = \sum_j \alpha_j \frac{d_j}{d} = \sum_j A_{ij}\alpha_j \tag{16}$$

which can be written as the matrix equation

$$\vec{\alpha}^* = \mathbf{A} \cdot \vec{\alpha} \tag{17}$$

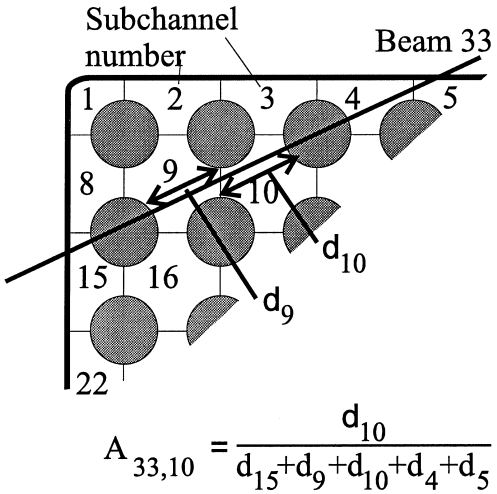

Fig. 3. Definition of matrix elements.

where the elements of $\vec{\alpha}^*$ are the measured chordal void-fractions and the elements of $\vec{\alpha}$ are the average void-fractions in each subchannel. To perform the tomographic reconstruction, this equation is inverted in the least-squares sense:

$$\vec{\alpha} = (\mathbf{A}^{\mathrm{T}}\Omega\mathbf{A})^{-1}\mathbf{A}^{\mathrm{T}}\Omega\vec{\alpha}^* \tag{18}$$

where Ω is a weighting matrix, which is best chosen as the inverted covariance matrix of the measurement errors. However, the covariance matrix of the measurement errors is not known, as only *chordal* void fractions are measured. Therefore, the identity matrix is used as the weighting matrix, which amounts to uniform weighting. In principle, the reconstruction can be improved by an iterative approach: the estimates of the *nodal* void fraction in the previous step can be used to get a better estimate of the weighting matrix Ω than a new reconstruction of the nodal void fraction can be made, etc. This iterative scheme has not been used in the present research. For the reconstruction to be possible, the matrix $\mathbf{A}^{\mathrm{T}}\mathbf{A}$ must be invertible. This means that there must be at least as many linearly independent chordal void-fraction measurements as there are subchannels. It is always possible to add an independent set of measurements by performing a scan under a different angle from the previous measurements. There are different ways to have exactly as many independent measurements as there are subchannels. However, it is more convenient to have more than this minimum number of measurements available. The precision of the reconstruction can be expressed as the covariance matrix of $\vec{\alpha}$ which is given by:

$$\mathrm{cov}(\vec{\alpha}, \vec{\alpha}) = (\mathbf{A}^{\mathrm{T}}\Omega\mathbf{A})^{-1}\mathbf{A}^{\mathrm{T}}\Omega\mathbf{V}\Omega\mathbf{A}(\mathbf{A}^{\mathrm{T}}\Omega\mathbf{A})^{-1} \tag{19}$$

where $\mathbf{V}$ is the covariance matrix of the errors in the measured data.

3.3. Data pre-processing

The tomographic reconstruction via Eq. (18) is the last step of the procedure which starts with measurement of the count rate by the detector. Before the tomographic reconstruction can be made, some operations are carried out on the measured data. This data pre-processing takes place in two steps.

3.3.1. Data acquisition and pre-processing part-1

- Place source and detector at the desired angle.
- Set the stepping motor in motion. The source and detector now scan the assembly at a constant speed.
- Collect the counts over short time intervals (e.g. 50 ms). This period is a compromise between two conflicting demands, which stem from the fact that we must take the logarithm of the count rate (Eq. (14)). The first demand is that there must always be at least one count in every sample, because we cannot take the logarithm of zero. This places a minimum on the sample rate. The second demand arises from the fact that the void-fraction fluctuates, and the average of the logarithm is not equal to the logarithm of the average. This means that the sample rate must be high enough to accommodate the void-fraction fluctuations.
- Stop the stepping motor.

- Correct the data for dead time of the detector and for the background.
- Calculate the logarithm of the sampled counts.
- Average the logarithms over a number of samples to obtain the desired spatial resolution.
- Correct for the decay of the gamma source and compare with a calibration measurement to calculate the relative logarithm of the count rate. All measurements are taken relative to a calibration measurement to eliminate changes in the source activity or any other long-term changes, for example, in the electronics.

In the present experiments, the sampling is done at a sample rate of 50 ms. At a moderate speed of the stepping motor the samples lie very close to each other, much closer than the collimator width. For each angle, chosen in step 1, 340–405 'chordal void fraction estimates' were obtained. These estimates are still subject to uncertainty due to the rather short sampling time and the fluctuating character of the flow (although the chordal averaging reduces the influence of fluctuations). Therefore, these estimates are resampled and averaged to yield 60 lines for a scan at a given angle, i.e. some nine estimates of the chordal void fraction per subchannel row (depending on the scanning angle). The result of the first pre-processing step is a signal of the relative logarithm of the count rate as a function of position. A few examples of such a signal are given in Fig. 4 for different angles of the gamma beam to the fuel assembly. If the gamma beam is at right angles to the fuel assembly, the six rows of fuel rods are clearly visible. At the left, we start outside the fuel assembly (count rate is maximal). Next, the gamma beam passes through the fuel assembly casing (minimum in count rate). Then, the count rate rises again and then falls as the gamma beam passes the first row of fuel rods. This is repeated for each row of fuel rods; with one row having a higher count rate than the rest. This is the row that contains the hollow 'water' rod.

At other angles, the fuel rods are not so clearly distinguishable. It is, however, always clear where the fuel assembly casing begins. This fact is used in the second step of the data pre-processing. The difference in the count rate for an assembly filled with liquid and an assembly filled with vapour shows where the fuel assembly casing stops and the flow begins. Another important conclusion from this figure is that the positioning system is not sufficiently accurate, since the two curves at angle 0 show a small horizontal offset (about 0.5 mm in this case). This small offset has a large effect on the difference between the two curves, which leads to a large error in the chordal void-fraction. It is the purpose of the second pre-processing step to eliminate this error.

3.3.2. Pre-processing part-2

- Locate the fuel assembly casing from the signal generated by pre-processing step 1. This is most easily accomplished by looking at the point where the signal passes below some value. This value should be chosen so that the location of the beam at this point lies well away from the location where the lines for the full and empty assembly start to diverge (say 0.5). The exact crossing point is interpolated from the surrounding data points. This is done for both sides of the fuel assembly.
- Scale the signal using the crossing points. The resulting signal crosses the assembly casing at 0 mm on one side. On the other side, it depends on the angle; for 0° the crossing point lies at 54 mm, for 15° at $54/\cos(15^\circ)$ mm, etc. (the width of the fuel assembly casing is assumed

to be exactly 54 mm).

- Resample the signal between the two crossing points by interpolation to obtain a limited number of chordal void-fractions for the tomographic reconstruction. The distance between two samples should be small enough so that each subchannel is passed by several beams for

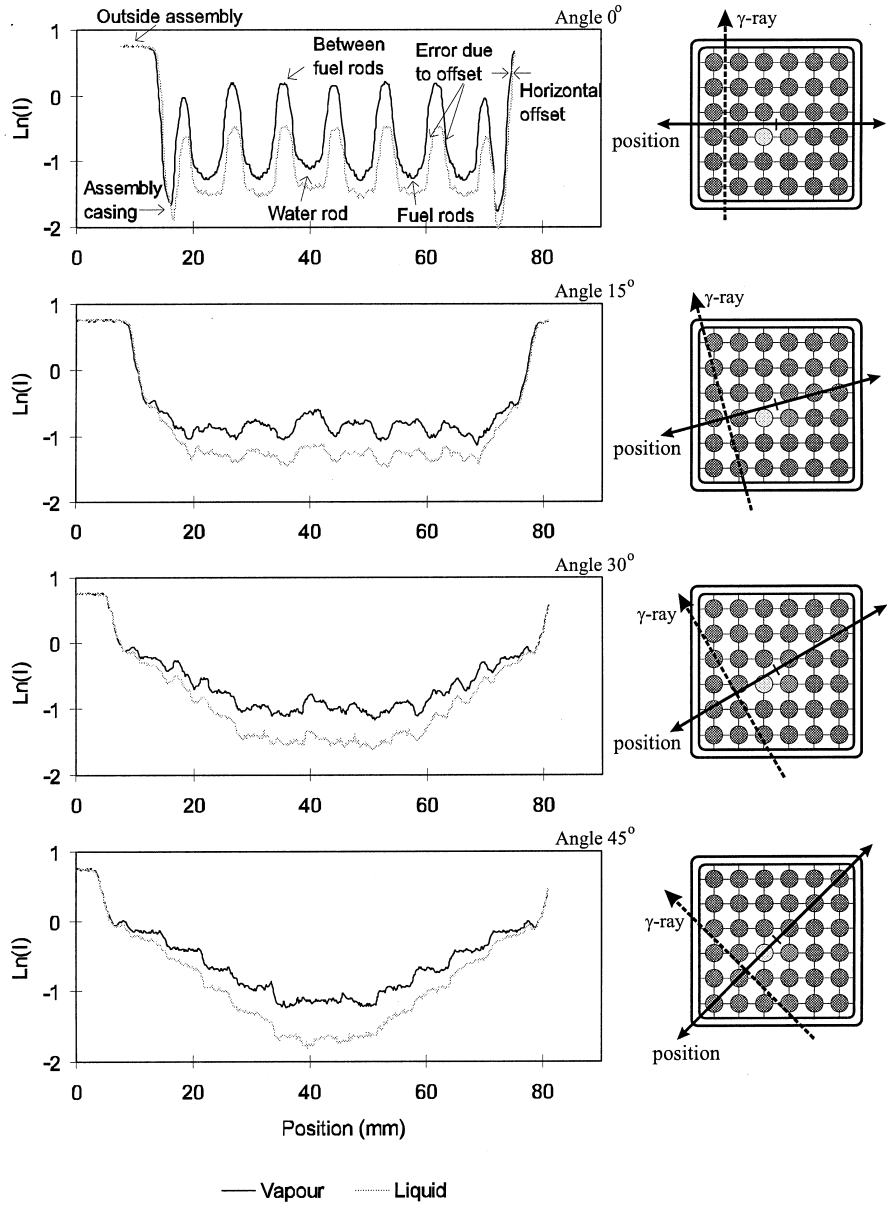

Fig. 4. Signal traces from the gamma detector at different angles to the fuel assembly. Shown are the logarithm of the countrate as a function of the linear position for an assembly filled with liquid and another filled with vapour. In the top of the figure the attenuating influence of the fuel rods is clearly visible.

each angle to achieve a good coverage of the subchannel. This averages out the effect of a non-homogeneous void-fraction distribution in each subchannel. Since the gamma beam has a width of 2 mm it is not useful to sample the signal with a much smaller sample distance.
- Calculate the chordal void-fraction at the sampled points using Eq. (14).

The two pre-processing steps are carried out for all angles at which a measurement was performed. This is the input to the tomographic reconstruction procedure. This procedure can handle an arbitrary number of entries of the above form. There is no constraint on the number or order of the entries. This means that it is possible to perform the reconstruction even if some of the measurements turned out later not to be successful.

3.4. Tomographic reconstruction

To perform the reconstruction, we need to calculate the elements A_{ij} which are the normalized distances of beam i travelled through node j. For this purpose, the fuel assembly is modeled as a rectangular box of 54×54 mm containing the fuel rods with diameters of 6.35 mm at a pitch of 8.8 mm. Deviations of the real assembly from this model due to rod flexing are not accounted for; these deviations are much smaller than the size of the subchannels and can be neglected. The model of the fuel assembly is described by a collection of straight lines and circles. From this model the distance of beam i through node j is calculated and normalized by the total length of beam i through the two-phase mixture. Finally, the void-fraction in the subchannels is calculated using Eq. (18).

4. The measurement set-up

4.1. The gamma source

The choice of the gamma source is mainly determined by the required energy of the gamma photons. This energy must be high enough so that the gammas penetrate the stainless steel casing, but not so high that they are not attenuated in the Freon. The variance in the measured void-fraction is partly caused by the statistical nature of the radioactive decay of the gamma source. The number of counts measured in a time interval has a Poisson distribution, thus the variance of the count rate is given by:

$$\sigma_I^2 = \frac{I}{t} \tag{20}$$

with t the measuring time. If we consider only the error in I (I_v and I_l can be measured with longer measuring times, since this needs to be done only once), then the standard deviation in the chordal void-fraction follows from Eqs. (14) and (20) as:

$$\sigma_{\alpha^*} = \frac{1}{\left(\mu_m d_m + \mu_l d_l + \mu_v d_v\right)\sqrt{It}} \tag{21}$$

This equation shows that the error in the chordal void-fraction depends on the gamma energy

(via the attenuation coefficient), on the length of the beam through the Freon and on the count rate. The count rate in turn is determined by the attenuation in the stainless steel casing, the Freon and the fuel rods; all of which are energy dependent. For DESIRE, the optimal energy lies around 300 keV. It was decided to use Cr-51 as source (emitting 320 keV gammas) because this could be produced cheaply in the nuclear research reactor of the IRI by irradiation of a piece of chromium of $2 \times 8 \times 8$ mm during 10 reactor days. This gives an activity of 276 mCi. To allow for the decay of short-lived isotopes, the piece is left to cool down for two days. These short-lived isotopes are formed by activation of small quantities of impurities in the chromium.

4.2. The set-up

The gamma source and detector are mounted on a translation table which is driven by a stepping motor. This translation table is mounted on a rotation table which can be rotated by hand (see Fig. 5). The whole system can be moved up and down along the assembly. The source is placed in the middle of a lead cylinder with a length of 10 cm and a diameter of 10 cm. A 5 cm long collimator with a cross-section of 2 mm horizontal and 8 mm vertical can be rotated in front of the source. At the detector side a shorter collimator of 1 cm length with the

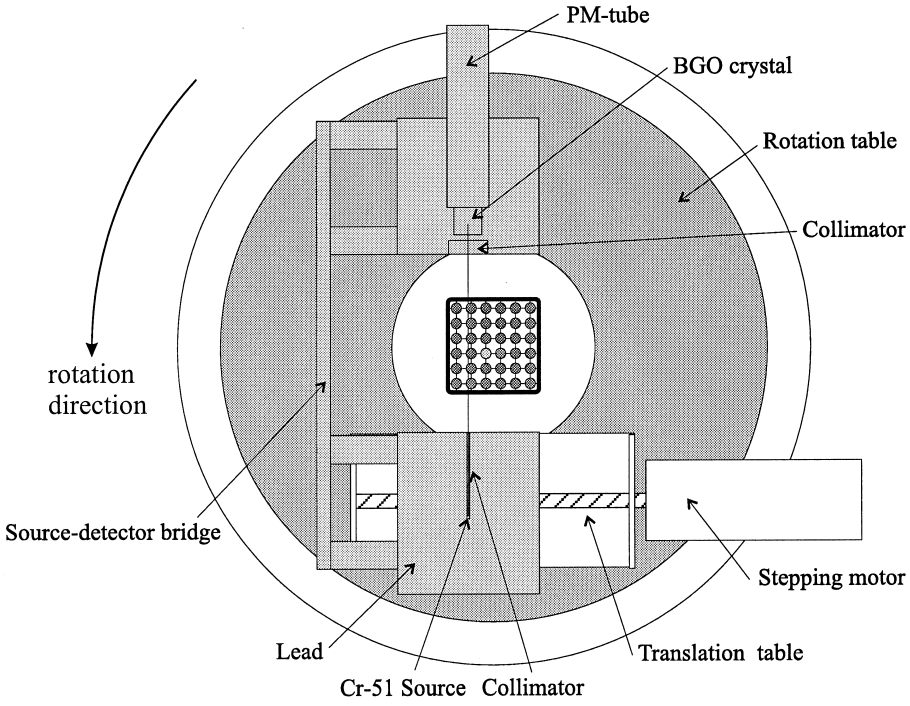

Fig. 5. The gamma-transmission set-up. The rotation table can be moved by hand, the translation table is moved by a stepping motor.

same cross-section is placed in front of the detector. These two collimators define a narrow beam of 2×8 mm.

The detector is a scintillation detector with a BGO (bismuth germanate, $Bi_4Ge_3O_{12}$) crystal as the scintillator. The light flashes from the scintillator are converted to a current and amplified in a photo-multiplier tube. The pulses from the photo-multiplier tube are further amplified, shaped and finally analyzed. The height of the pulses is a direct measure for the amount of energy that was deposited in the scintillator crystal by the gamma photon (only the pulses in the photo peak are counted). The pulses from the amplifier are first passed through a spectrum stabilizer. A single channel analyzer converts the pulses that fall within a window placed around the photo peak to standard pulses which are counted by a data-acquisition board in a PC.

4.3. Error analysis

There are many conceivable sources for error in the reconstructed void-fraction. Some of the errors can be corrected, some can be calculated, but others can only be speculated upon without a detailed study.

4.3.1. Errors due to the Poisson statistics of the gamma source

Eq. (19) can be used to determine how the error in the measured chordal void-fraction affects the error in the reconstructed void-fraction. The error in the chordal void-fraction due to the Poisson statistics is determined by the number of counts, the void-fraction and the location of the gamma beam. The number of counts was typically 10,000. This leads to an error varying from 0.02 to 0.12. Using 12 angles and a total of more than 700 chordal void-fractions, this gives an error in the order of 0.004 in the reconstructed void-fraction for the center subchannel, about 0.01 in the wall subchannels and 0.02 in the corner subchannels (absolute errors).

4.3.2. Errors due to counting of gamma photons of higher energy which give pulses in the 320 keV photo-peak via Compton interaction with BGO

It was found that there were impurities in the chromium which became activated when the piece was irradiated. As a result gamma photons of various energies were emitted. Since the attenuation coefficient is different for these gamma photons, they must not be counted by the detector. This cannot be avoided for those gamma photons which undergo a Compton interaction in the scintillator crystal resulting in a pulse that falls in the 320 keV photo peak. This is the reason that BGO was chosen as a scintillator crystal; it has a very good photo peak efficiency. Also, it was found that letting the chromium cool off some extra few days after irradiation substantially reduced the problem.

4.3.3. Error in positioning of the source-detector

This problem was discussed in the previous section. It has been solved using the data pre-processing.

4.3.4. Fuel rod bending

In the reconstruction procedure, the lengths of the gamma rays passing through the subchannels is calculated. In this calculation, the fuel rods are assumed to be at their correct position. However, it is clear from visual inspection that the fuel rods are not perfectly straight, so that their position varies with height. If a fuel rod is displaced into a certain subchannel, then the void-fraction in that subchannel will be underpredicted. Fortunately, since this means that the fuel rod is displaced out of the subchannel to the opposite of this subchannel, the void-fraction in this subchannel will be overpredicted. In general, these errors will almost cancel so that the average void-fraction is not affected by fuel rod bending.

4.3.5. Deviations of the real geometry from the assumed geometry

The walls of the fuel assembly casing are not exactly flat, due to the high pressure inside. Also the corners of the fuel assembly casing are rounded. These effects are not accounted for in the reconstruction procedure, although this is principally possible. Especially for the corner subchannels, which have a small area, this has a large effect. This, in combination with the problem of measuring very close to the fuel assembly casing makes the measurement in the corner subchannels less reliable than in the other subchannels.

4.3.6. Uncertainty analysis

The reliability of the measured data should be subjected to an uncertainty analysis. However, a standard 'propagation-of-errors' technique cannot be applied, as the standard deviation in the nodal estimates is not known (nodal void fractions are not known, only *chordal* averages are measured). More research is needed in this area, we will focus on this in future work.

5. Void-fraction measurements

A total of nine measurement runs were performed. During each run the subchannel void-fractions were measured at six heights along the assembly (at 16, 28, 40, 52, 64 and 76 cm). The spacers are located at 25, 49 and 73 cm, so the measurements were taken at least 3 cm downstream of the spacers. Local disturbances of the void-fraction due to the spacers are not to be expected at this distance. Takenaka used neutron radiography to measure the void-fraction in the region around the spacers. He found that the void-fraction decreased by some four percentage points at the spacer itself, but the void-fraction downstream of the spacer returned to an equilibrium value within 1 cm (Takenaka, 1996). Table 1 gives the operating conditions for the measurement runs. The pressure during all the runs was nominal (11.6 bar). The measurements are divided into three series (A, B and C in the table). The first series entailed a variation of the power at constant flow rate. The second series consists of one measurement at reduced flow rate. The third series is a variation of the radial power profile, going linearly from flat to tilted.

The reconstruction of the void-fraction distribution in the subchannels at a given height is based on 12 scans. After each scan the rotation table holding the source and detector is rotated over an angle of 15° (i.e. from 0° to 165°).

The results are shown in Figs. 6 and 7. The 35 fuel rods are shown as black circles and the water rod as a black circle with a white dot inside. Some general features apparent from these figures are the presence of the water rod, where the void-fraction is lower than average, and the effect at the walls of the fuel assembly, where the void-fraction also is lower than average.

5.1. The cross-sectional average void-fraction

Fig. 8 shows the cross-sectional average void-fraction compared to two models: the homogeneous model without subcooled boiling and the drift-flux model with subcooled boiling using Dix's correlation. The agreement with the latter model is excellent. However, it is instructive to give a qualitative comparison of the measurements with the homogeneous model.

At the lowest measuring point of 16 cm the measured void-fraction is much higher than the void-fraction according to the homogeneous model. This is caused by subcooled boiling. The thermodynamic equilibrium quality at this point is almost zero. Between 16 and 28 cm the thermodynamic equilibrium quality is positive. At some point, thermodynamic equilibrium will be reached and the flow quality will be equal to the thermodynamic equilibrium quality. At the point where thermodynamic equilibrium is reached, the vapour will still be concentrated near the rod walls. Since the velocity of the flow is lower at this location, the distribution parameter will be smaller than unity. Also, the bubbles will still be small and the local drift velocity will be small. In such a case, the drift-flux model predicts a void-fraction which is higher than the void-fraction in the homogeneous model. This is the case between the first two measuring points. As the flow develops, the bubbles move into the center of the subchannels. The distribution parameter becomes larger than unity and the local drift velocity increases. These two effects cause the void-fraction to be lower than the void-fraction according to the homogeneous model. In all measurements there is a dip in the void-fraction at the third measurement point at a height of 40 cm. The origin of this dip is unknown, but one of the following factors could play a role:

- *Spacer effect*: The second and fourth measurement points lie just 3 cm above the first and second spacer, respectively. If the spacer causes an increase in the void-fraction just downstream, this would partly explain the dip in the third measurement point which does

Table 1
DESIRE operating conditions during measurements

Measurement run	Power (kW)	Flow (kg/s)	Subcooling (°C)	Power profile
A1	15	1.6	0.5	Flat
A2	30	1.6	0.8	Flat
A3	40	1.6	1.0	Flat
B	22	1.16	1.7	Flat
C1	22	1.6	1.0	Flat
C2	22	1.6	1.0	Tilted (550–710) W/rod
C3	22	1.6	1.0	Tilted (470–780) W/rod
C4	22	1.6	1.0	Tilted (380–880) W/rod
C5	22	1.6	1.0	Tilted (300–970) W/rod

not lie in the neighborhood of a spacer.

- *Error in the calibration measurement*: For all the measurement series, the same calibration measurements of I_l and I_v in Eq. (14) are used. Although these measurements were carried out with care, a measurement error at the third measurement height would affect all measurement series in the same way.
- *Flow pattern transition*: A transition from bubbly flow to a churn or annular like flow would decrease the void-fraction after the transition. The maximum possible void-fraction for a bubbly flow lies at about 30%. This could explain the dip in most measurements. However, this hypothetical flow pattern transition takes place between the second and third measurement point in all measurements, irrespective of the void-fraction in this region which

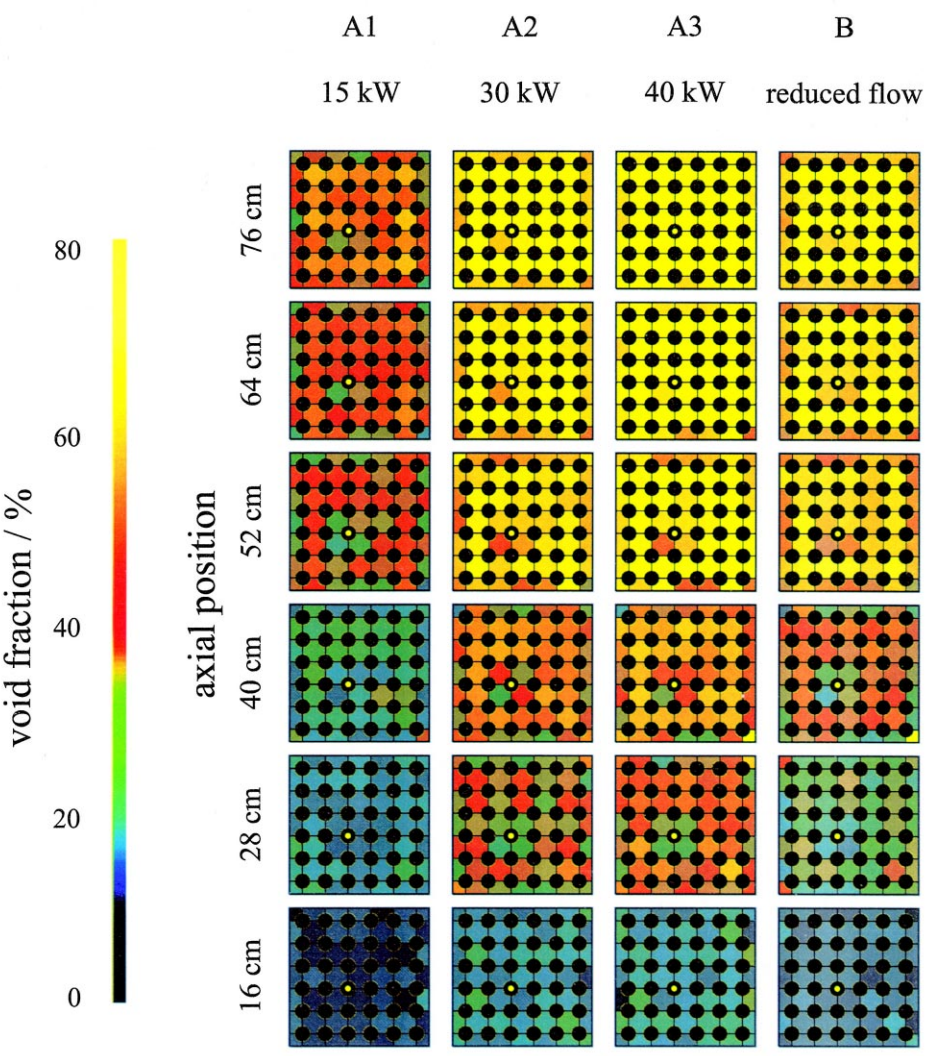

Fig. 6. Subchannel void-fraction at six heights for various measurements.

varies from ±25 to ±40%. This makes the flow pattern transition as an explanation for the dip not fully convincing. However, there is evidence of a flow pattern transition from measurements of the void-fraction distribution within the subchannels (see below). This transition also occurs at a height between 30 and 40 cm, irrespective of the void-fraction.

5.2. The void-fraction in different subchannels

There are several types of subchannel in the fuel assembly. We can identify subchannels at the corner, at the wall and center subchannels. All these have a different geometry. Among the center subchannels there are four subchannels next to the 'water' rod. The void-fraction

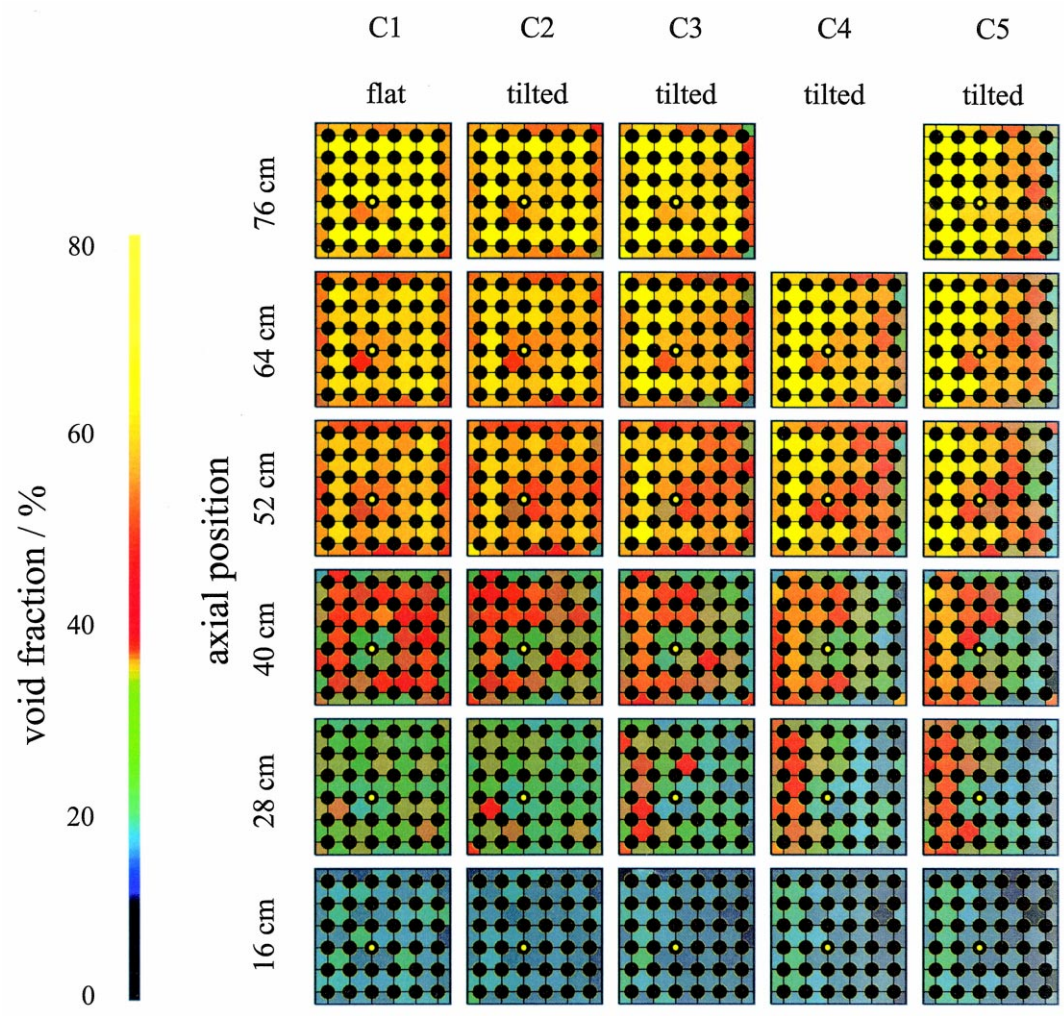

Fig. 7. Subchannel void-fraction at six heights for various measurements.

development in these different types of subchannel is shown in Fig. 9, where the corner and wall subchannels have been grouped into a single group (called the periphery). In the left column of Fig. 9 the development of these void-fractions along the height of the subchannel is shown.

This must be compared with the power that goes into each channel. It is assumed that one-quarter of the power produced by each fuel rod surrounding the subchannel goes into that

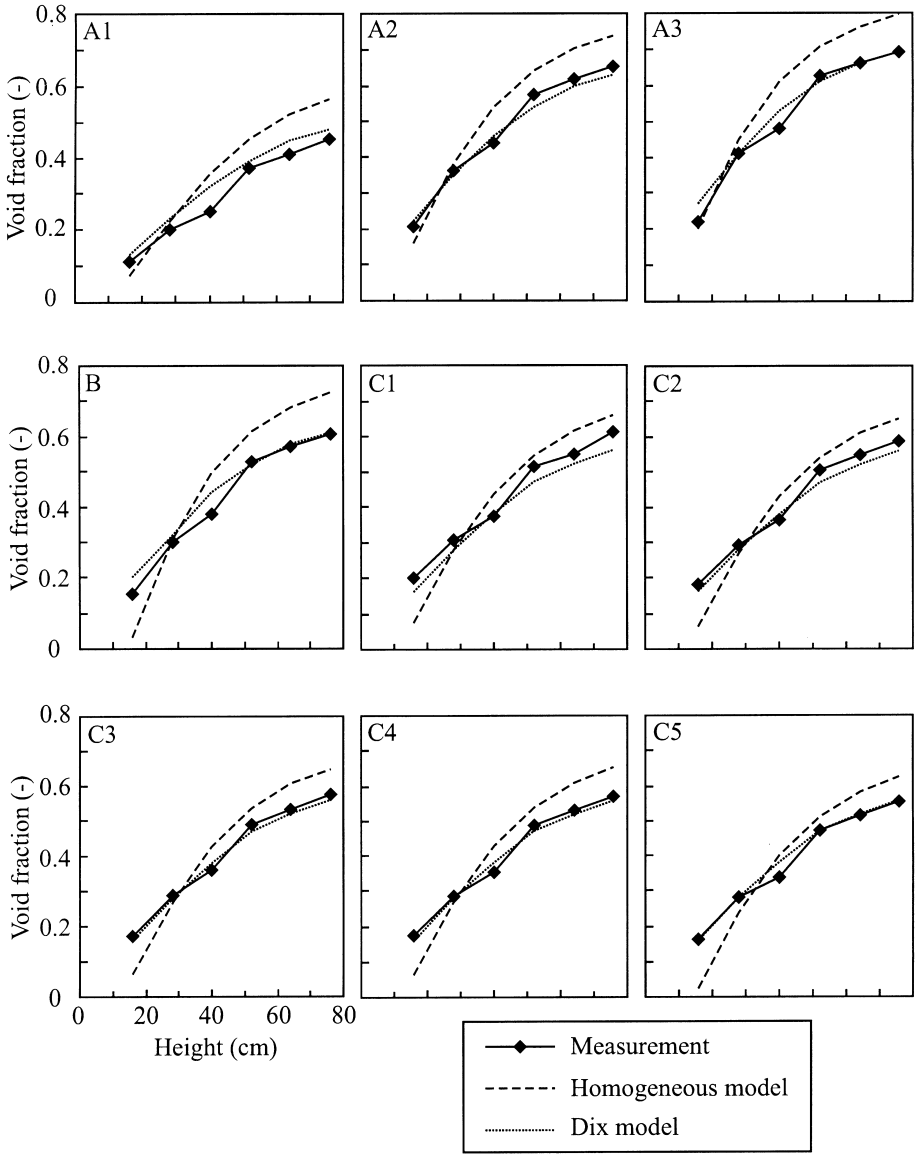

Fig. 8. Cross-sectionally averaged void-fraction as a function of the height compared with the homogeneous model and the drift-flux model using Dix's correlation.

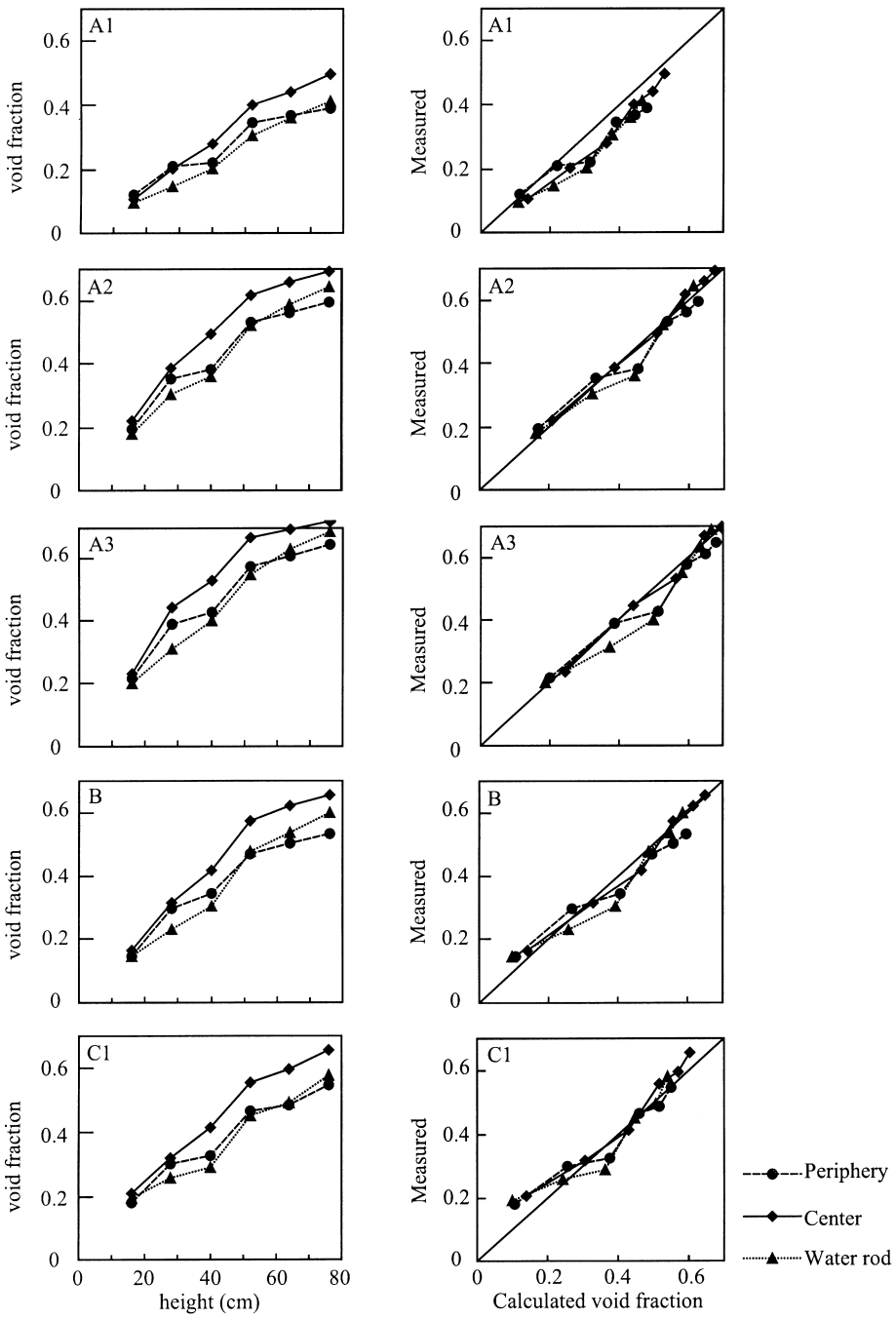

Fig. 9. Void-fraction in the different subchannel types as a function of height (left) and compared with the drift-flux model (right).

subchannel. The power/flow-area ratio of the peripheral subchannels is 82% of the power/flow-area ratio of the center subchannels. One striking fact is that at the bottom of the assembly, the void-fractions in the center and peripheral subchannels are about equal, despite the different power/flow-area ratios. It may be that the flow rate in the peripheral subchannels is lower. Above 40 cm height the void-fraction in the peripheral subchannels is lower than in the center subchannels. To determine if void transport between the subchannels takes place, we apply the drift-flux model to each subchannel individually (again Dix's correlation is used, although strictly speaking this correlation is derived for bundles and not for subchannels). The calculated results are compared with the measurement results in a scatter plot in the right column of Fig. 9. If there was void transport taking place, the lines in this scatter plot would diverge for the different types of subchannels. In all plots a slight divergence can be seen at higher void-fractions. The measured void-fraction for the periphery consistently lies below the line for the center subchannels which indicates transport of void from the periphery to the center. The differences, however, are quite small. Another indication of void transport from the periphery to the center is that the void-fraction of the center subchannels adjacent to the wall subchannels is larger than the void-fraction in the other center subchannels (see Figs. 6 and 7 and the curve for C1 in Fig. 10, which has a maximum at the second and sixth row). Unlike the peripheral subchannels the subchannels next to the water rod have the same geometry as the other center subchannels. The lines for the center and water subchannels in the scatter plots do not diverge. Even at higher void-fractions the two lines lie close to each other. Thus, there seems to be little transport of vapour from the center into the water subchannels.

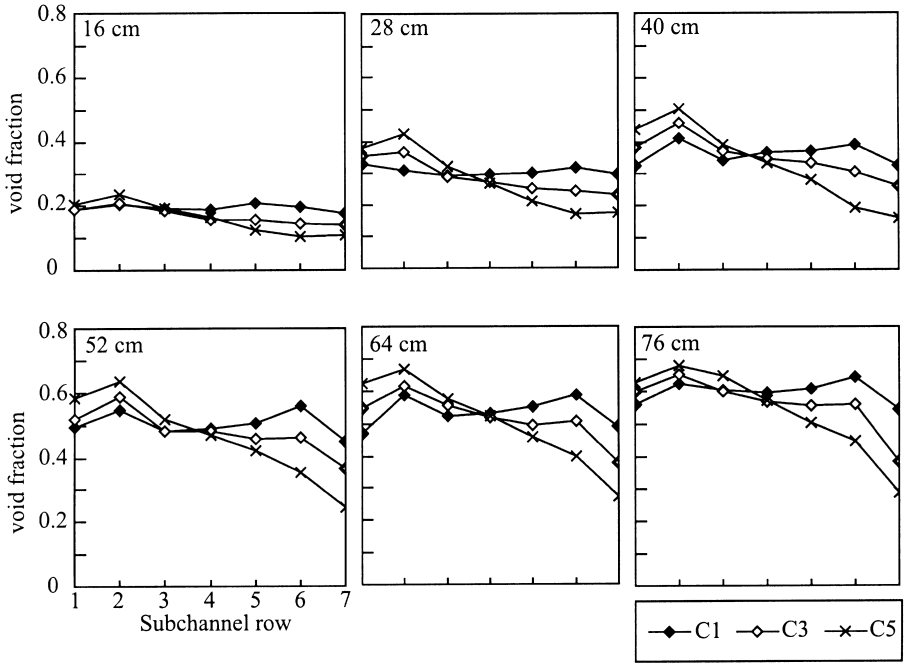

Fig. 10. The effect of a titled power profile on the lateral void-fraction distribution: the power decreases linearly from subchannel row 1 to 7.

5.3. Void-fraction with a tilted power profile

Net lateral void transport, if it were to occur, should particularly be visible in the measurement with the tilted power profile. In Fig. 10 the void-fraction averaging over subchannels of equal power (again it is assumed that one-fourth of the power of each fuel rod forming the subchannel is put into that subchannel) is shown at the six measuring heights. In Fig. 11 a scatter plot is shown comparing the measured void-fraction to the calculated void-fraction using the drift-flux model and the assumption of no vapour transport between subchannels. As can be seen the two are in good agreement.

If vapour is transported from subchannels with a higher void-fraction to subchannels with a lower void-fraction, this would have an equalizing effect on the measured void-fraction. The slope of the lines in Fig. 11 connecting all measurement points at the same height will then

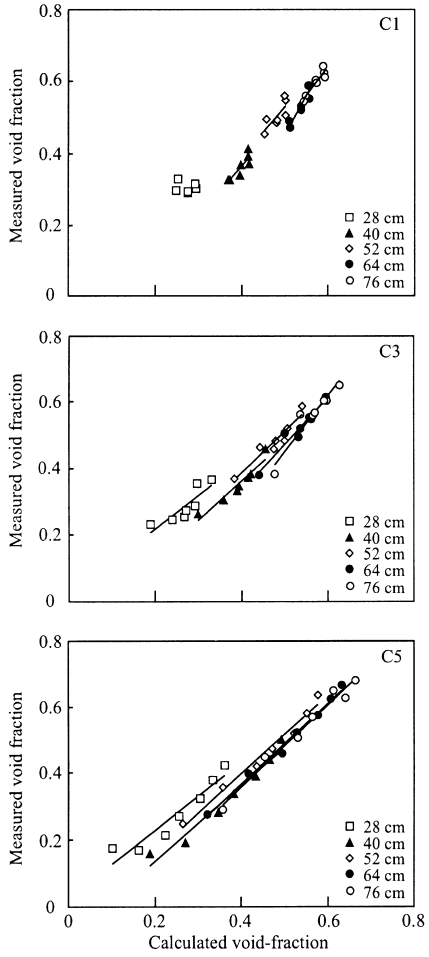

Fig. 11. Comparison of measured versus calculated void-fraction using the drift-flux model with Dix's correlation.

decrease. This is not the case, so it is concluded that on an assembly-wide basis the void-fraction follows the power profile.

5.4. Void-fraction distribution within the subchannels

All the results presented upto this point were based on the tomographic reconstruction of the void-fraction in the subchannels. In this reconstruction, it is assumed that the void-fraction in each subchannel is distributed homogeneously. This is obviously a wrong assumption, since the bubbles at the bottom are created at the rod walls while in a developed flow the vapour is concentrated in the center. Since each subchannel is traversed by many gamma beams at different angles and positions, all points within each subchannel are equally sampled, so the effect of the non-homogeneous distribution is averaged out in the result. However, closely examining the signal from the detector, signs of this non-homogeneous distribution could be found. This is clearly illustrated by performing a simple comparison between the chordal void-fraction as measured exactly between the fuel rods or as measured exactly through the fuel rods (see Fig. 2). The latter probes only the gap region between the rods. The former probes both the gap and the center region of the subchannels. The difference between these two reflects the difference of void-fraction in the bulk of the flow in the center of the subchannel and in the flow close to the fuel rods. The results are shown in Fig. 12. A clear transition can be seen in the figure, where the void-fraction in the bulk increases more rapidly than the void-fraction near the fuel rods. This is indicative of a transition from bubbly flow to annular flow

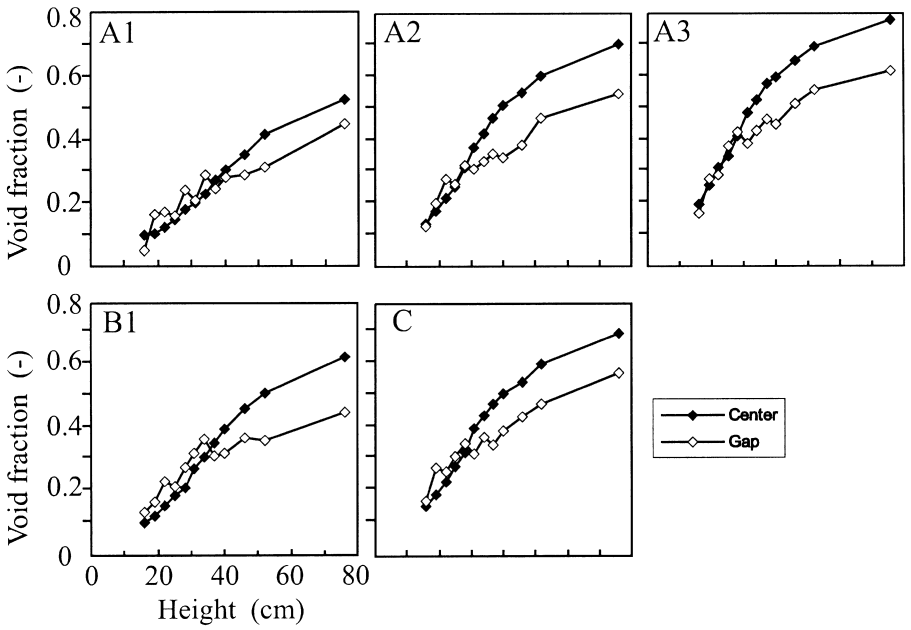

Fig. 12. Chordal void-fraction along two beams shown in Fig. 2 as a function of the height.

in each subchannel. As discussed, this transition could be the reason for the dip in the average void-fraction at the third measuring point at a height of 40 cm (Fig. 8).

6. Conclusions

A relatively simple subchannel void-fraction measurement system is developed and applied to a scaled model of a BWR fuel assembly that uses Freon-12 as a coolant. The measurement system is based upon the gamma-transmission technique and uses a tomographic reconstruction procedure to calculate the void-fractions in the subchannel. Three measurements must be performed for each chordal void-fraction: one with the assembly filled with liquid, one with the assembly filled with vapour and one with the assembly in operation. Each time the gamma beam must be located at exactly the same position. Instead of using a very accurate and complex positioning system, we use data pre-processing to remove the positioning errors. Measurements were performed under different operating conditions and radial power profiles. The measurements are compared with the drift-flux model in combination with Dix's correlation. The measured average void-fraction is in good agreement with the model. At one measurement height, the measured void-fraction is lower than expected (for all measurement runs). Several possible reasons for this discrepancy are discussed. The void-fraction in the wall and corner subchannels is lower than the average which can be explained by the fact that the power/flow area ratio is smaller for these subchannels. By applying the drift-flux model to each subchannel separately and comparing with measurements, the presence of lateral void-drift should be detectable. No evidence for lateral void-drift was found except near the top of the assembly. By comparing two chordal void-fractions, a flow pattern transition could clearly be seen between a void-fraction of 30% and 40%. This transition is characterized by an increase of the void-fraction in the center of the subchannels relative to the void-fraction close to the fuel rods, which corresponds to a transition from bubbly to an annular flow pattern.

References

Dix, G.E., 1971. Vapour Void Fractions for Forced Convection with Subcooled Boiling at Low Flow Rates. NEDO-10491 General Electric Company.

Inoue, A., 1995. Void-fraction distribution in a boiling water reactor fuel assembly and the evaluation of subchannel analysis codes. Nuclear Technology 112, 388–400.

Kok, H.V., van der Hagen, T.H.J.J., Mudde, R.F., 1995. Investigations on the thermal-hydraulics of a natural circulation cooled BWR fuel assembly. In: Proc. of NURETH-7 Conference, September 10–15, Saratoga Springs, New York, vol. 4, 2884–2894.

Kok, H.V., 1998. Experiments on a Natural Circulation Loop — From Void-fraction to Coupled Nuclear Thermal–Hydraulic Dynamics. Ph. D. Thesis, Delft University of Technology, The Netherlands.

Lahey, R.T., 1990. The analysis of phase separation and phase distribution phenomena using two-fluid models. Nucl. Eng. Des 122, 17–40.

Lahey, R.T., Moody, F.J., 1993. The Thermal–Hydraulics of a Boiling Water Nuclear Reactor. American Nuclear Society.

Natterer, F, 1982. The Mathematics of Computerized Tomography. Verlag B.G. Teubner, Stuttgart.

Saha, P., Zuber, N., 1974. Point of net vapor generation and vapor void fraction in subcooled boiling. In: Proc. 5th Int. Heat Transfer Conf., vol. 4, 157–179.

Schrock, V.E., 1969. Radiation attenuation techniques in two-phase flow measurements. In: Eleventh National ASME/AiChe Heat Transfer Conference, Minneapolis, 24–35.

Takenaka, N., 1996. Three dimensional void fraction measurement of two-phase flow in a rod bundle by neutron radiography. Nucl. Instr. and Methods in Physics A 377, 115–118.

Tanke, R.H.J., Jasper, J.E., Gaalman, P.A.M., Killian, D., 1991. Application of Tomography in Nuclear Research, Kerntechnik 56.

Van de Graaf, R., van der Hagen, T.H.J.J., Mudde, R.F., 1994a. Scaling laws and design aspects of a natural circulation cooled simulated boiling water reactor fuel assembly. Nuclear Technology 105, 190–200.

Van de Graaf, R., van der Hagen, T.H.J.J., Mudde, R.F., 1994b. Two-phase scaling laws for a simulated BWR assembly. Nucl. Eng. Des 148, 455–462.

Yadigaroglu, G., Maganas, A., 1995. Equilibrium quality and mass flux distribution in BWR fuel assembly and evaluation of subchannel codes. Nuclear Technology 122, 455–462.

Yagi, M., Mitsutake, T., Morooka, S., 1992. Void-fraction distribution in BWR fuel assembly and evaluation of subchannel analysis code. In: Proc. Int. Sem. Subchannel Analysis, The Institute of Applied Energy, October 30, Tokyo, Japan.